Molecular Structure of the Rat Vitamin D Receptor Ligand Binding Domain Complexed with 2-Carbon-Substituted Vitamin D3 Hormone Analogues and A LXXLL-Containing Coactivator Peptide

5 AUTHORS, INCLUDING:

John Wesley Pike
University of Wisconsin–Madison

243 PUBLICATIONS **12,379** CITATIONS

Molecular Structure of the Rat Vitamin D Receptor Ligand Binding Domain Complexed with 2-Carbon-Substituted Vitamin D₃ Hormone Analogues and a LXXLL-Containing Coactivator Peptide[†,‡]

Janeen L. Vanhooke,*,‖ Matthew M. Benning,§ Cary B. Bauer,§ J. Wesley Pike,‖ and Hector F. DeLuca*,‖

Department of Biochemistry, University of Wisconsin−Madison, 433 Babcock Drive, Madison, Wisconsin 53706, and Bruker AXS Inc., 5465 East Cheryl Parkway, Madison, Wisconsin 53711

Received November 17, 2003

ABSTRACT: We have determined the crystal structures of the ligand binding domain (LBD) of the rat vitamin D receptor in ternary complexes with a synthetic LXXLL-containing peptide and the following four ligands: $1\alpha,25$-dihydroxyvitamin D_3; 2-methylene-19-nor-($20S$)-$1\alpha,25$-dihydroxyvitamin D_3 (2MD); 1α-hydroxy-2-methylene-19-nor-($20S$)-bishomopregnacalciferol (2MbisP), and 2α-methyl-19-nor-$1\alpha,25$-dihydroxyvitamin D_3 (2AM20R). The conformation of the LBD is identical in each complex. Binding of the 2-carbon-modified analogues does not change the positions of the amino acids in the ligand binding site and has no effect on the interactions in the coactivator binding pocket. The CD ring of the superpotent analogue, 2MD, is tilted within the binding site relative to the other ligands in this study and to ($20S$)-$1\alpha,25$-dihydroxyvitamin D_3 [Tocchini-Valentini et al. (2001) *Proc. Natl. Acad. Sci. U.S.A. 98,* 5491−5496]. The aliphatic side chain of 2MD follows a different path within the binding site; nevertheless, the 25-hydroxyl group at the end of the chain occupies the same position as that of the natural ligand, and the hydrogen bonds with histidines 301 and 393 are maintained. 2MbisP binds to the receptor despite the absence of the 25-hydroxyl group. A water molecule is observed between His 301 and His 393 in this structure, and it preserves the orientation of the histidines in the binding site. Although the α-chair conformer is highly favored in solution for the A ring of 2AM20R, the crystal structures demonstrate that this ring assumes the β-chair conformation in all cases, and the 1α-hydroxyl group is equatorial. The peptide folds as a helix and is anchored through hydrogen bonds to a surface groove formed by helices 3, 4, and 12. Electrostatic and hydrophobic interactions between the peptide and the LBD stabilize the active receptor conformation. This stablization appears necessary for crystal growth.

The physiologically active form of vitamin D_3 is $1,25$-$(OH)_2D_3$[1] (illustrated in Figure 1, along with the analogues discussed below). This seco-steroid hormone functions within target cells of the bone, kidney, and intestine to maintain circulating calcium and phosphorus concentrations at levels required for proper skeletal mineralization and neuromuscular function (*1*). The hormone has also been demonstrated to have suppressive effects on the immune system (*2*), to promote cellular differentiation, and to inhibit cellular proliferation (*3−6*). $1,25$-$(OH)_2D_3$ is used clinically to treat renal osteodystrophy, vitamin D dependency rickets type I, and X-linked hypophosphatemic rickets (*7−10*). As the biological actions of $1,25$-$(OH)_2D_3$ have become better understood, this hormone and its analogues have been intensively investigated for use in treating a variety of other conditions and diseases, including osteoporosis, psoriasis, autoimmune disease, and malignancies of the breast and prostate (*11−15*). Clinical use of $1,25$-$(OH)_2D_3$ for these purposes has often been limited, however, because therapeutic doses can give rise to significant hypercalciuria and hypercalcemia (*12, 16, 17*).

A multitude of vitamin D_3 analogues have been synthesized in recent years in an attempt to provide beneficial therapeutic agents with low calcemic activity. Chemical modifications of every portion of the vitamin D_3 molecule (the A, C, and D rings, the 17β-aliphatic side chain, and the 5,6,7,8-diene moiety) have been reported (*18−20*). Over the past 5 years, Sicinski et al. have reported the synthesis of several 2-substituted, 19-norvitamin D_3 analogues with high

* To whom correspondence should be addressed. E-mail: deluca@biochem.wisc.edu and jlvanhoo@wisc.edu.

‖ University of Wisconsin−Madison.

§ Bruker AXS Inc.

[1] Abbreviations: $1,25$-$(OH)_2D_3$, $1\alpha,25$-dihydroxyvitamin D_3; 2MD, 2-methylene-19-nor-($20S$)-$1\alpha,25$-dihydroxyvitamin D_3; 2MbisP, 1α-hydroxy-2-methylene-19-nor-($20S$)-bishomopregnacalciferol; 2AM20R, 2α-methyl-19-nor-$1\alpha,25$-dihydroxyvitamin D_3; CCD, charge-coupled display; DBD, DNA binding domain; DRIP, vitamin D receptor-interacting protein; DTT, dithiothreitol; EDTA, ethylenediaminetetraacetic acid; EPPS, *N*-(2-hydroxyethyl)piperazine-*N'*-3-propanesulfonic acid; HPLC, high-pressure liquid chromatography; IPTG, isopropyl-β-D-thiogalactopyranoside; LB, Luria Bertani; LBD, ligand binding domain; LBDM, rat VDR−LBD($\Delta165$−211); MOPS, 3-(*N*-morpholino)propanesulfonic acid; NR, nuclear receptor; PEG, poly(ethylene glycol); PPARγ, peroxisome proliferator-activated receptor gamma; RXR, retinoid X receptor; SDS−PAGE, sodium dodecyl sulfate polyacrylamide gel electrophoresis; SRC-1, steroid receptor coactivator-1; TR, thyroid hormone receptor; TRAP, thyroid hormone receptor-associated proteins; Tris, Tris(hydroxymethyl)aminomethane; VDR, vitamin D receptor.
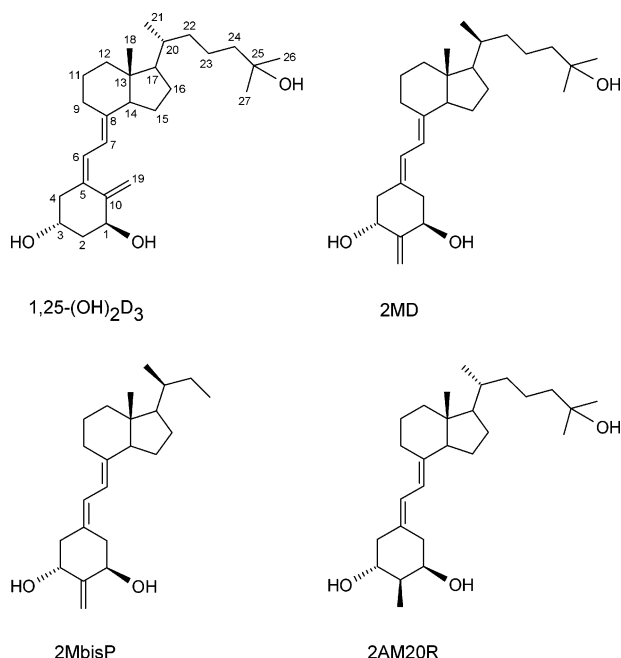
FIGURE 1: Chemical structures of the ligands used for the crystal structure determinations.

biological activity (*21, 22*). One of these analogues, 2MD, has demonstrated tremendous therapeutic potential (*23*). 2MD is a highly potent stimulator of HL-60 promyelocyte differentiation in vitro. In vivo, this analogue exhibits preferential activity on the bone, stimulating calcium resorption from the skeleton with at least a 30-fold greater potency than the natural hormone. Normally such high calcemic activity might be expected to render an analogue useless for pharmacotherapy, but unlike the natural hormone and other vitamin D_3 analogues developed to date, 2MD also promotes the synthesis of new bone, and it does so at doses that do not adversely affect serum calcium levels (*23*). At present, this analogue is in the early stages of clinical testing for use in the treatment of osteoporosis.

Two structural features distinguish 2MD from the natural hormone: the A-ring methylene moiety is transposed from C10 to C2, and the stereochemical configuration at C20 of the side chain is inverted to that of the *S* stereoisomer. Very recently, DeLuca and co-workers have prepared a series of 2-methylene, 19-norvitamin D_3 analogues with shortened aliphatic side chains (manuscript in preparation). The analogue 2MbisP has the same A-ring modification and stereochemical inversion as 2MD but is truncated at C23 and contains no hydroxyl group at the end of the aliphatic chain. 2MbisP stimulates the in vitro differentiation of promyelocytes with slightly less activity than 1,25-$(OH)_2D_3$. It has no calcemic activity in either the bone or the intestine in vivo, even at high doses, though it demonstrates in vivo activity in its ability to suppress the level of circulating parathyroid hormone. These findings suggest that 2MbisP may prove useful for the treatment of proliferative diseases and/or secondary hyperparathyroidism.

The physiological actions of 1,25-$(OH)_2D_3$ are mediated through the VDR, a nuclear hormone receptor that functions as a ligand-dependent transcriptional modulator. The VDR binds 1,25-$(OH)_2D_3$ with very high affinity; reported dissociation constants range from 0.01 nM (*24*) to 0.70 nM (*25*). Binding of 1,25-$(OH)_2D_3$ promotes the formation of a heterodimeric complex of VDR and RXR on cognate DNA elements in the promoters of target genes (*26*). Hormone binding also appears to drive a conformational transition at the carboxy terminus of the VDR, creating a binding surface that facilitates interaction of the receptor with coactivator proteins that further modulate transcription through chromatin remodeling and recruitment of the basal transcription machinery (*27–29*). A number of coactivators have recently been described, including those of the p160 family and the DRIP/TRAP complex (*29*). These proteins interact with the VDR through a nuclear receptor binding motif that contains an LXXLL consensus sequence (*29, 30*).

The 2-substituted vitamin D_3 analogues also bind tightly to the VDR, 2MD with an affinity that is approximately equal to the natural hormone (*21*), and 2MbisP at approximately 10-fold less (manuscript in preparation). We have undertaken the three-dimensional structural determination of the VDR as a means of establishing whether the differences in biological potency and tissue selectivity of these compounds can be attributed to perturbations in the VDR structure or its interactions with coactivators. The VDR has proven to be one of the most difficult nuclear receptors to crystallize. The first structural determinations of the receptor were reported by Moras and co-workers (*31, 32*), who obtained crystals of liganded complexes of the human VDR–LBD upon removal of 50 amino acids that comprise a highly flexible surface loop. We have created the corresponding deletion in the LBD of the rat VDR and cocrystallized this protein with a synthetic peptide containing the LXXLL sequence of the coactivator DRIP 205 (*33*), along with the ligands 1,25-$(OH)_2D_3$, 2MD, and 2MbisP. In addition, we have also crystallized the LBDM·peptide complex with 2AM20R, a 2α-methyl-substituted analogue for which the conformational equilibrium of the A ring is shifted and highly favors the α-chair form (*21*). The structural analysis of these complexes is presented in this paper.

EXPERIMENTAL PROCEDURES

Materials. Chemically competent *Escherichia coli* BL21-Codon Plus (DE3)-RIL cells were obtained from Stratagene. Ultrafiltration membranes and centrifugal devices for protein concentration were products of Millipore. Ni–NTA Super-flow and SP–Sepharose Fast Flow were obtained from Qiagen and Amersham Pharmacia, respectively. The synthetic peptide used in the crystallization experiments was prepared at the University of Wisconsin–Madison Biotechnology Center, and each lot of peptide was purified by HPLC and analyzed by mass spectroscopy prior to use. 1,25-$(OH)_2D_3$, 2MD, and 2MbisP were supplied by Deltanoid Pharmaceuticals Inc. (Madison, WI). 2AM20R was synthesized by Sicinski as previously described (*21*).

Protein Expression and Purification. The protein used for this investigation was expressed in *E. coli* BL21-Codon Plus (DE3)-RIL cells harboring the plasmid p29LBDM. This plasmid is a derivative of pET-29b (Novagen) and codes for the production of the rat VDR–LBD (residues 116–423) lacking the flexible insertion region (residues 165–211) and containing a hexahistidine tag at the carboxy terminus. Cells were cultured with vigorous agitation at 37 °C in LB medium supplemented with kanamycin and chloramphenicol. Once A_{600} reached 0.8–1.0, the culture was rapidly chilled to ~23

°C. IPTG was then added to a final concentration of 50 μM, and agitation was resumed at 22−24 °C for 6 h. The cells were pelleted by centrifugation and scooped into liquid nitrogen. This procedure typically yielded 6 g of cell paste/L of culture.

All purification procedures were performed at 4 °C. The clarified extract obtained after cell lysis (sonication) and centrifugation was incubated with 20 mL of Ni−NTA Superflow chromatographic resin for 1 h. The slurry was subsequently packed into a column (2.5 cm diameter), and the resin was washed thoroughly with 50 mM Tris at pH 8.0, containing 0.5 M NaCl, 10% glycerol, 5 mM β-mercaptoethanol, and 10 mM imidazole. LBDM was eluted from the resin by increasing the imidazole concentration in the buffer to 150 mM. The eluate from the metal affinity column was dialyzed against 20 mM sodium phosphate at pH 7.0, containing 1 mM EDTA, 5% glycerol, and 2 mM DTT, after which it was applied to a 2.5 × 12 cm column of SP−Sepharose Fast Flow. After a wash to remove the nonbinding proteins, LBDM was eluted from the cation exchange column with a gradient of NaCl that linearly increased from 0 to 0.5 M in phosphate buffer over a total volume of 400 mL. Fractions judged pure by SDS−PAGE were combined and concentrated to 0.5−1.0 mg/mL by ultrafiltration (YM10 membrane). The concentrated protein was dialyzed against 10 mM Tris at pH 7.0, containing 10 mM DTT and 0.02% NaN$_3$. The yield of LBDM from this procedure was typically 2.5−3.0 mg/L of cell culture. The ligand binding activity of the receptor was quantitated by a modified hydroxyapatite assay with radiolabeled 1,25-(OH)$_2$D$_3$ (*34*). Scatchard analysis of the data yielded an equilibrium dissociation constant (K_d) of 0.37 nM (data not shown).

Complexation with the Ligands and LXXLL-Containing Peptide. All ligands were dissolved in absolute ethanol, and their concentrations were determined spectrophotometrically before use. The ligands were added to aliquots of the purified protein in a 10-fold molar excess, in a volume that established a final ethanol concentration of 2%. These complexes were allowed to sit on ice for 1−2 days, after which the protein was concentrated to 5−6 mg/mL in centrifugal concentrating devices. The synthetic peptide, of the amino acid sequence KNHPMLMNLLKDN−NH$_2$, was prepared as an 8.5 mM solution in 25 mM EPPS at pH 8.0, containing 50 mM NaCl, 2 mM DTT, and 0.02% NaN$_3$. This peptide was added to the concentrated LBDM·ligand complexes in a 5-fold molar excess over the protein. The ternary complexes were allowed to sit on ice for at least 2 h prior to their use in the crystallization experiments.

Crystallization of the LBDM·Ligand·Peptide Complexes. Crystallization trials were conducted by the hanging drop method of vapor diffusion at 4 °C using the Crystal Screen Lite, Crystal Screen 2, and Memb Fac crystallization screening kits of Hampton Research. Thin diamond-shaped crystals were obtained from several test solutions containing PEG. The crystal habit was significantly improved by additional screening in hanging drops at room temperature. Crystals ultimately used for the structural analysis described here were grown at room temperature by macroseeding from hanging drops into small batch setups. For these experiments, the ternary complex was quickly mixed with an equal volume

Table 1: Unit Cell Dimensions and Data Collection Statistics

ligand	1α,25-(OH)$_2$D$_3$	2MD	2MbisP	2AM20R
unit cell dimensions				
a (Å)	154.73	154.60	154.45	154.80
b (Å)	44.15	43.29	44.11	42.29
c (Å)	42.07	41.85	41.86	41.79
β (deg)	96.13	96.07	96.62	96.15
resolution (Å)	30.0−2.20	30.0−1.99	30.0−1.90	30.0−2.28
completeness (%)	99 (95)[a]	99 (96)	99 (90)	90 (70)
redundancy	5.7	4.9	4.8	3.7
ave I/ave $\sigma(I)$	10.9 (2.7)	10.8 (3.5)	20.8 (3.4)	14.1 (4.2)
R_{factor} (%)[b]	5.2 (19.8)	5.1 (16.1)	3.2 (15.3)	4.5 (14.9)

[a] Values in parentheses are for the highest resolution shell. [b] R_{factor} = $(\sum|I − \bar{I}|/\sum I) \times 100$.

of a precipitant solution composed of 26−30% PEG 4000, 100 mM MOPS (pH 7.0), 200 mM ammonium citrate (pH 7.0), and 4% 2-propanol. Drops of 15 μL were pipetted into greased nine-well Plexiglas depression plates and carefully seeded thereafter. Diamond-shaped crystals of various dimensions were obtained from these conditions in approximately 2 weeks; those employed for data collection were typically 0.20 × 0.20 × 0.075 mm. These crystals were determined to belong to the monoclinic space group *C*2; unit cell dimensions for the crystals of each complex are listed in Table 1.

X-ray Data Collection and Processing. Prior to X-ray data collection, the crystals were rapidly transferred in a stepwise fashion to a cryoprotectant solution composed of 18% PEG 4000, 100 mM MOPS (pH 7.0), 200 mM ammonium citrate (pH 7.0), 5 mM DTT, 2% 2-propanol, and 20% ethylene glycol. The crystals were then suspended in small nylon loops and flash cooled to −160 °C in a stream of nitrogen gas. An X-ray data set was collected from a single crystal of each complex. The X-rays were generated with a Bruker Nonius FR591 generator, and the reflections were recorded on a Bruker Nonius Proteum R CCD detector. X-ray exposure times ranged from 1 to 2 min/deg (0.3 deg/image), with a crystal-to-detector distance of 5.0 cm. The crystals diffracted well in all directions to 2.0 Å resolution; anisotropic diffraction was observed at higher resolution. The X-ray data were processed with the programs SAINT and ProScale, from the Proteum software suite (Bruker AXS Inc.). Relevant X-ray data collection statistics are given in Table 1.

Computational Methods. Structural determination and refinement of the LBDM·ligand·peptide complexes were performed using programs from the CCP4 crystallographic program suite (*35*). The structure of the complex containing 2MD was solved by molecular replacement with the program MOLREP (*36*). The protein coordinates of the human VDR−LBD(Δ165−215)·1,25(OH)$_2$D$_3$ complex served as the search model for this procedure. The molecular replacement solution had a correlation of 46.1% and an *R* factor of 49.0%. The *R* factor was reduced to 29.7% following 5 cycles of maximum likelihood refinement with the program REFMAC (*37*). The protein model was fit into the electron density map using TURBO FRODO (*38*). After several cycles of refinement, the ligand, peptide, and solvent molecules were positioned into the map. Alternate cycles of maximum likelihood refinement and model fitting were subsequently performed to generate the final model of the complex. The structures of the complexes containing 1,25-(OH)$_2$D$_3$, 2MbisP, and

Table 2: Refinement Statistics

ligand	$1\alpha,25\text{-}(OH)_2D_3$	2MD	2MbisP	2AM20R
R_{cryst}[a]	19.0	18.5	19.3	18.0
R_{free}[b]	24.3	24.4	22.6	21.8
RMS bond length (Å)	0.016	0.015	0.016	0.016
RMS bond angles (deg)	1.38	1.39	1.38	1.46
protein atoms	1897	1907	1922	1915
peptide atoms	91	83	84	79
ligand atoms	30	30	25	30
solvent molecules	92	133	125	68
average B factor (Å^2)				
protein main chain	33.22	29.01	28.96	28.66
peptide main chain	46.78	41.70	38.82	41.46
ligand	25.53	20.64	23.54	19.74
solvent	41.03	39.30	39.16	34.06

[a] R_{factor} values are calculated as $\sum|F_o - F_c|/\sum|F_o|$, where F_o and F_c are the observed and calculated structure factor amplitudes, respectively. [b] R_{free} is calculated with a test data set containing a random selection of 5% of the observed reflections.
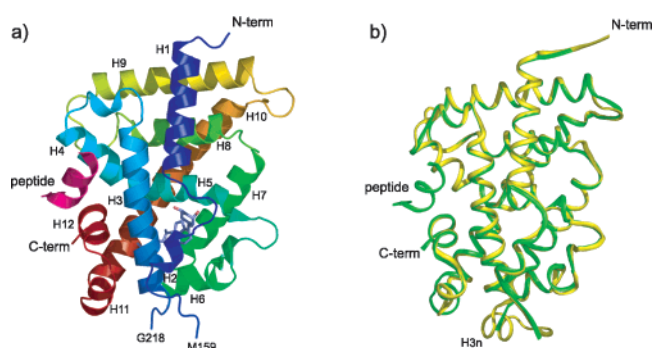

FIGURE 2: Molecular architecture of the rat VDR−LBD and comparison to the human homolog. (a) Ribbon representation of the rat LBDM·2MD·peptide complex. Helix numbering of the protein is based on that for the human retinoid X and retinoic acid receptors (28, 49). The synthetic peptide is shown in magenta, and 2MD is illustrated in stick format. (b) Superposition of the rat LBDM·2MD·peptide (green) and the human VDR−LBD(Δ165−215)·1,25-(OH)$_2$D$_3$ (yellow) complexes (ligands not shown). The orientation of the drawing is identical to that in panel a. This figure and Figures 3−6 were produced using the program PyMOL (50).

2AM20R were solved by difference Fourier techniques, with the protein coordinates from the LBDM·2MD·peptide complex serving as the initial model. Relevant refinement statistics are presented in Table 2. The stereochemical quality of the models was assessed by use of the program PROCHECK (39). Ramachandran plots show no significant outliers; 94% of the residues are in the most-favored regions, and the remainder, in allowed regions. All superpositions described in the following section were performed with the program LSQKAB (40).

RESULTS

Overall Protein Structure. The four crystalline complexes are isomorphous; thus, once the initial molecular replacement solution was obtained, subsequent structures could easily be solved by the difference Fourier method. A ribbon representation of the LBDM·2MD·peptide complex is shown in Figure 2a. The observed protein conformation is identical in each complex; the main-chain atoms of the 2MD-, 2MbisP-, and 2AM20R-containing complexes superimpose on those of the 1,25-(OH)$_2$D$_3$-containing complex with root-mean-square deviations of 0.18, 0.20, and 0.23 Å, respectively. In each structure, the visible electron density com-

mences at Lys 123 and terminates at Asn 420. There is a structural break between helices 2 and 3; amino acids 160−164 and 212−217, which flank the deletion, are disordered, and no corresponding electron density is observed in the maps. In the complex with 2MbisP, Gly 419 and Asn 420, which lie just beyond helix 12, are modeled into the electron density in two conformations. In the other complexes, the electron density maps suggest the second conformation is also present for these two amino acids; however, the density is weak and is modeled with solvent molecules.

As described for the human VDR−LBD (31), the LBD of the rat receptor folds into an α-helical sandwich, with the ligand buried within the core. The backbone Cα atoms of the rat and human proteins superimpose with a root-mean-square deviation of 0.53 Å. A superposition of the structures is shown in Figure 2b. Both proteins assume the "closed" conformation, with helix 12 positioned against the protein such that it seals the ligand binding site, and along with helices 3 and 4, creates a hydrophobic binding cavity for interaction with a coactivator protein. The synthetic LXXLL-containing peptide used in this study binds within this cavity in each of the four complexes (Figures 2a and 5a). The structure of the human receptor was determined in the absence of any added peptide. In this structure, the hydrophobic cavity is filled by a short helix (H3n, Figures 2b and 5b) from a symmetry-related molecule.

Ligand Binding Interactions. The ligand binding sites for 2MD and 2MbisP are superimposed on that for 1,25-(OH)$_2$D$_3$ in parts a and b of Figure 3, respectively. Both panels of the figure illustrate that the positions of the amino acid residues within the binding site are virtually identical in the three complexes. The most remarkable differences are observed in the ligand conformations. The natural ligand binds as previously reported for the human receptor, in an extended conformation that is anchored by π−π interactions between Trp 282 and the 5,6,7,8-diene and by six hydrogen-bonding interactions: Ser 233 and Arg 270 with the 1α-OH; Tyr 143 and Ser 274 with the 3-OH; His 301 and His 393 with the 25-OH. As compared to the natural ligand, 2MD shares a very similar conformation for the A ring and the 5,6,7,8-diene. The CD ring of 2MD, however, is notably tilted. The combination of this tilting and the inverted configuration at C20 directs the 17β-aliphatic chain along a different path within the binding site. Nevertheless, the 25-OH moiety at the end of the chain occupies the same position as that of the natural ligand, and as such, all hydrogen-bonding interactions are preserved. In contrast to 2MD, the conformation of the entire core portion of 2MbisP closely resembles that of 1,25-(OH)$_2$D$_3$, with only a very slight tilt observed for the CD ring. Carbons 22 and 23 of the truncated aliphatic side chain occupy positions that are significantly different from those of 1,25-(OH)$_2$D$_3$; however, their positioning is accommodated within the binding pocket with no change in the conformation of the neighboring amino acid residues. An ordered water molecule (B factor = 26.9 Å^2) is present in the 2MbisP binding site in the position normally occupied by the 25-OH of the natural ligand. This water molecule maintains the hydrogen bonds that are observed with His 301 and His 393. The distances between the hydrogen-bonding partners in each of the binding sites are listed in Table 3.

Table 3: Comparison of Selected Interatomic Distances

atom	neighbor	atomic distance (Å)		
		1,25-(OH)$_2$D$_3$	2MD	2MbisP
1α-OH	Ser 233 OG	2.76	2.76	2.61
	Arg 270 NH1	2.83	2.90	2.89
3-OH	Tyr 143 OH	2.67	2.72	2.81
	Ser 274 OG	2.95	3.04	2.89
25-OH	His 301 NE2	2.85	2.70	
	His 393 NE2	2.70	2.76	
wat3[a]	His 301 NE2			2.83
	His 393 NE2			2.80
C19	Leu 229 CG	3.97		
	Leu 229 CD1	3.95		
	Ser 233 OG	3.42		
	Ile 267 CG2	3.66		
C28[b]	Tyr 143 CE2		3.85	3.83
	Phe 150 CZ		3.98	3.88
	Arg 270 NH1		3.61	3.67
	wat1		3.76	3.73
	wat2		3.51	3.65
C11	Leu 226 CD2	4.26	3.99	3.99
C16	Met 268 CG	4.08	3.82	4.13
	Leu 309 CD2	4.24	3.89	4.07
C18	Val 230 CG2	3.53	3.72	3.57
C21	Ile 264 CD1	5.41	3.93	4.78
	Leu 305 CD2	3.72	4.10	3.98
	His 393 CD2	4.22	3.84	3.95
C22	His 301 CD2	4.73	4.40	3.88
C23	Leu 226 CB	5.72	6.04	3.98
	Val 230 CG2	4.28	4.10	3.87
	His 301 NE2	3.64	3.60	4.24
	His 301 CD2	3.84	3.90	4.01
	His 393 NE2	3.93	3.66	5.81
	His 393 CD2	4.27	3.94	6.00

[a] wat3 is the designation of the solvent molecule between His 301 and His 393 in the 2MbisP structure. [b] C28 is the designation assigned to the 2-methylene carbon of the analogues.

A distance cutoff of 4.0 Å was used to assign the neighboring residues for each binding site. Because of the differences in their chemical composition and binding conformation, the 2-substituted analogues have neighbors that differ somewhat from each other and from those of 1,25-(OH)$_2$D$_3$. To fully compare the environment of the binding sites, the superpositions in Figure 3 include the total set of neighbors for 1,25-(OH)$_2$D$_3$ and the specific 2-methylene analogue. Phe 150 and the two water molecules near the A ring are beyond the cutoff distance in the 1,25-(OH)$_2$D$_3$ binding site but are included in each panel of the figure because they neighbor the 2-methylene carbon of 2MD and 2MbisP. The methylene carbon of 1,25-(OH)$_2$D$_3$ is located at position 10 of the A ring and neighbors Leu 229 and Ile 267; neither of these amino acid residues is within 4.0 Å of 2MD or 2MbisP. The tilting of the CD ring of 2MD brings Leu 226, Ile 264, Met 268, and Leu 309 within the cutoff range and takes Leu 305 out of neighboring distance. Leu 226 also neighbors 2MbisP, because of the slight tilt of the ring system and the different positioning of C23. The list of selected interatomic distances presented in Table 3 allows further inspection of the neighbor differences. From the data, it can be seen that despite the obvious tilt of the CD ring of 2MD, the distances between the atoms of the ring and the nearby amino acid residues do not differ greatly from those of 1,25-(OH)$_2$D$_3$ and 2MbisP. For example, the distance between C16 of 2MD and Cγ of MET 268 is 3.82 Å; in the 1,25-(OH)$_2$D$_3$ and 2MbisP structures, this distance is 4.08 and 4.13 Å, respectively. The side-chain positions of the ligands result in larger differences in the neighboring atom distances, especially for C21 of 2MD and C21−C23 of 2MbisP.

Table 3 also lists the protein and solvent atoms within 4.0 Å of the 2-methylene carbon (C28) of 2MD and 2MbisP. The extra carbon is accommodated without any obvious disruption in the structure of the protein or the ordered solvent molecules observed in the vicinity. The interactions of the 2-methylene carbon with the neighboring atoms appear to be limited to hydrophobic and van der Waals contacts. The aromatic side chains of Tyr 143, Tyr 147, and Phe 150 all surround the A ring; however, none are positioned appropriately for a π-bond-stacking interaction with the ligand.

Ligand A-Ring Conformation. The A ring of 1,25-(OH)$_2$D$_3$ and the 2-methylene-substituted analogues can assume two chair conformations in solution. These conformers, denoted α and β, equilibrate rapidly and are present in nearly equimolar concentrations (*21*, *41*). In the crystal structures, the β conformer is observed exclusively for these ligands, and in this conformation, the 1α-OH group is equatorial (Figure 3). The conformational equilibrium for the 2α-methyl-substituted analogue, 2AM20R, is shifted and predominately favors the α-chair conformation, which has an axial 1α-OH group. (*21*). We prepared the crystalline complex with this analogue in order to assess whether the VDR is able to bind ligands with the A ring in the α conformation. The electron density for the 2AM20R ligand is shown in Figure 4a, and from the map, the β conformation of the A ring is unambiguously assigned. The 1α-OH group is equatorial, and the 2α-methyl substituent occupies the energetically unfavorable axial position. All hydrogen bonds between the protein and the A-ring hydroxyl groups are maintained in the binding site (data not shown).

Peptide Binding Interactions. The amino acids of the LXXLL-containing peptide (KNHPMLMNLLKDN−NH$_2$) are identical to amino acids 625−637 of the coactivator DRIP 205 (*33*), and for simplicity, the peptide is assigned the same sequence numbering. This sequence contains the second nuclear receptor-interacting motif of the coactivator (the "NR-2 box") and effectively competes with DRIP 205 for interaction with the VDR (*33*). Electron density is observed for the peptide in each complex between Asn 626 and Lys 635. The peptide folds as a short helix and, as indicated earlier, binds in a surface groove formed by helices 3, 4, and 12. This interaction buries approximately 507 Å^2 of the receptor's surface area [calculated with the CCP4 routine SURFACE (*42*, *43*), using a probe sphere radius of 1.4 Å]. A close-up view of the peptide in the binding pocket is depicted in Figure 5a. Binding-site interactions are contributed by Ile 238, Lys 242, Phe 247 (helix 3), Ser 252, Gln 255, Ile 256, Leu 259, Lys 260 (helix 4), Pro 412, Leu 413, and Glu 416 (helix 12). The carboxylate oxygens of Glu 416 accept hydrogens from the main-chain amides of Met 629 (2.89 Å) and Leu 630 (2.87 Å), and the ε-amino group of Lys 242 donates a hydrogen to the main-chain carbonyl of Leu 633 (3.23 Å). These interactions form a "charge clamp" analogous to that previously described for the interaction between the nuclear receptor PPARγ and the coactivator SRC-1 (*44*). The side chains of leucines 630, 633, and 634 of the LXXLL motif are buried within the pocket and surrounded by hydrophobic amino acids. The nonspecific
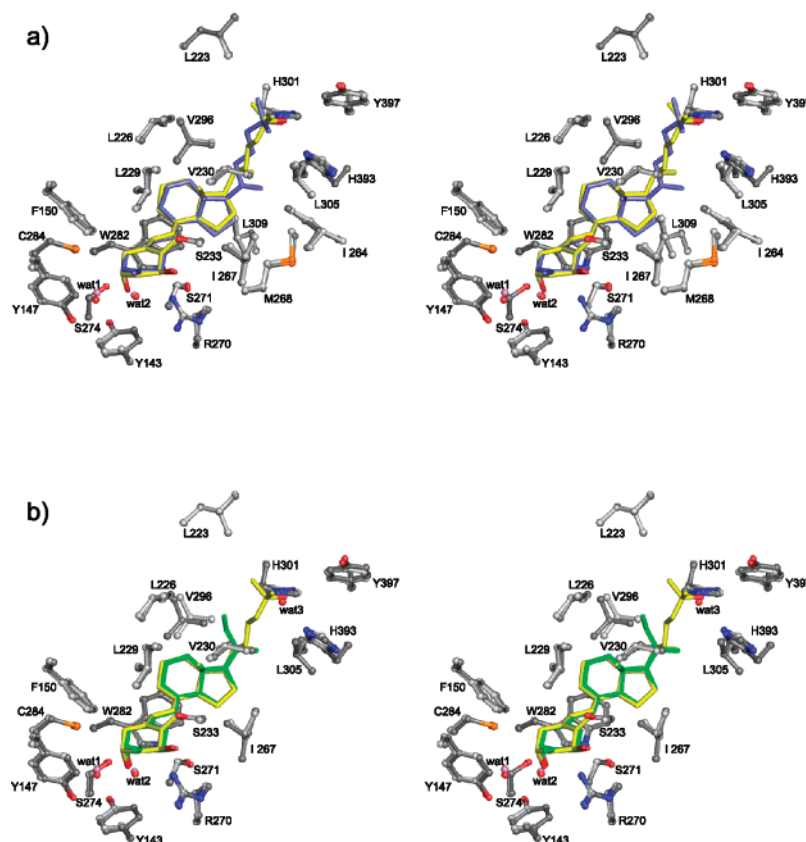
FIGURE 3: Stereoviews of superpositions comparing the binding site of 1,25-(OH)$_2$D$_3$ with that of 2MD (a) and 2MbisP (b). 1,25-(OH)$_2$D$_3$ is depicted in yellow in both panels; 2MD and 2MbisP are slate blue and green, respectively. Hydroxyl moieties of the ligands are colored red. In each panel, amino acid residues located within 4.0 Å of either 1,25-(OH)$_2$D$_3$ or the analogue are shown in a ball-and-stick format, with carbons of the residues in the 1,25-(OH)$_2$D$_3$ binding site colored light gray and those in the analogue sites colored dark gray. Two water molecules (wat1 and wat2) neighbor the 2-substituent of the analogues; these molecules are shown as red spheres, and the corresponding water molecules in the 1,25-(OH)$_2$D$_3$ binding site are shown in pink. The additional water molecule (wat3) observed in the 2MbisP binding site between H301 and H393 is also displayed in panel b as a red sphere.
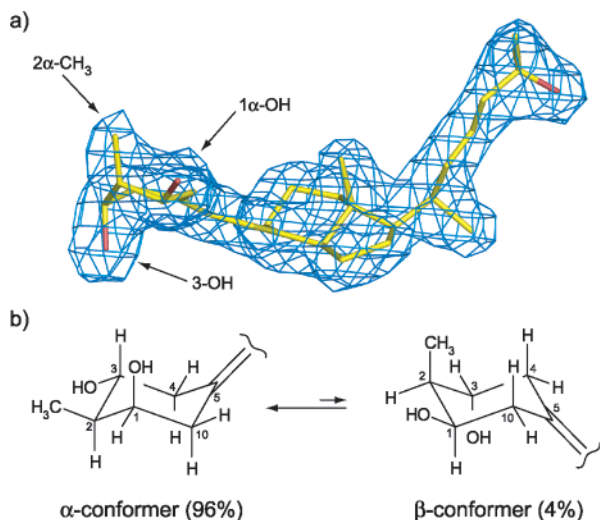

FIGURE 4: Ligand A-ring conformation in the LBDM·2AM20R· peptide complex. (a) 2F_o − F_c electron density for 2AM20R, contoured at 1σ. The 1α-OH, 3-OH, and 2α-CH$_3$ groups are indicated with arrows. (b) Structure and solution equilibrium of the A-ring conformers of 2AM20R.

amino acids of the motif, Met 631 and Asn 632, are directed away from the binding cavity and out toward the solvent. This type of orientation for the LXXLL region is also observed in the PPARγ·SRC-1 crystal structure (*44*).

In the crystal structure of the human VDR−LBD, the coactivator binding pocket is filled by a short helix contrib-uted by a protein molecule that is related by crystallographic symmetry. This helix, denoted H3n, has the sequence S$_{216}$-VTLELSQL$_{224}$, and its interaction in the binding pocket is presented in Figure 5b for comparison. The H3n helix is anchored through a charge clamp with Glu 420 and Lys 246, which correspond to Glu 416 and Lys 242 in the rat VDR. One of the carboxylate oxygens of Glu 420 forms a hydrogen bond with the side-chain hydroxyl group of Ser 216 (2.48 Å). The other is positioned to accept a hydrogen from either the side-chain hydroxyl group or the main-chain amide nitrogen of Thr 218 (the distances of these interactions are 2.79 and 2.67 Å, respectively). The ϵ-amino group of Lys 246 donates a hydrogen to the main-chain carbonyl oxygen of Ser 222 (2.78 Å). From the structural comparison, it is determined that the sequence corresponding to L$_{630}$MNLL$_{634}$ is T$_{218}$LELS$_{222}$. Cγ of Thr 218 and the aliphatic side chain of Leu 221 are directed into the binding pocket and mimic several of the hydrophobic interactions of Leu 630 and Leu 633. None of the hydrophobic interactions of Leu 634 are available for the side chain of Ser 222, and it is directed away from the surface of the binding pocket.

DISCUSSION

From the data presented here, we conclude that the differences in the biological activity of the 2-carbon-modified analogues are not reflected in the three-dimensional structure of the LBD of the VDR. The binding cavity for the ligand is quite large, and the protein accepts the structural modifica-
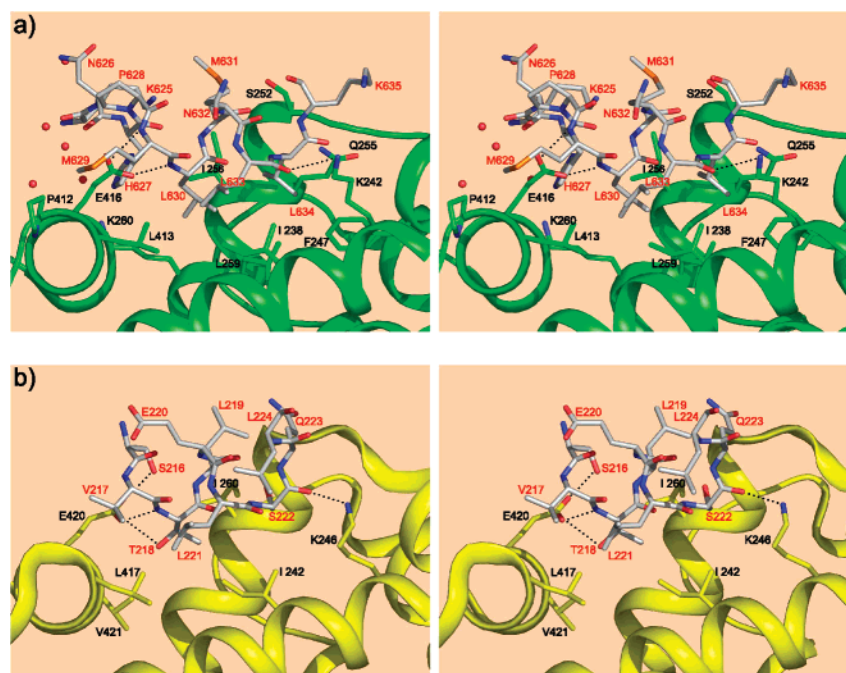
FIGURE 5: Close-up stereoviews of the coactivator binding pockets of the rat and human VDR−LBDs complexed with 1,25-(OH)$_2$D$_3$. (a) Interaction between the synthetic LXXLL-containing peptide and the rat receptor. (b) Interaction between the H3n helix and the human receptor. In both panels, the peptide is shown in Corey−Pauling−Koltun-colored sticks, with the individual amino acid residues labeled in red. The receptors are shown as ribbons, with side chains of the amino acid residues located within 4.0 Å of the peptide displayed and labeled in black. Water molecules neighboring the peptide in panel a are shown as red spheres. Key hydrogen bonds that position the peptides are denoted with dotted lines.

tions at C2 and in the aliphatic side chain without any conformational disruption. This conclusion is not unlike that reached by Moras and co-workers in their study of the human VDR−LBD. The crystal structures of the human receptor with 1,25-(OH)$_2$D$_3$ and the side-chain-modified analogues MC1288 (20S-1α,25-dihydroxyvitamin D$_3$) and KH1060 (1α,25-dihydroxy-(20S)-22-oxa-24,26,27-trihomovitamin D$_3$) also revealed that the receptor conformation is unaffected, with differences observed only in the ligand orientations (*32*).

The 17β-aliphatic side chain is permitted substantial flexibility within the binding site, which allows the 25-OH of 2MD, MC1288, and KH1060 to establish the same hydrogen bonds that are observed for the natural ligand, even though the chains course different paths. It is interesting to note here that while the side chains of 2MD and MC1288 have the same stereochemical configuration and chemical composition, some of the torsion angles along the chains differ significantly. This difference arises because of the increased tilting of the CD ring of 2MD relative to MC1288 and is illustrated in Figure 6. These analogues exert similar effects on cellular differentiation, but 2MD is much more active on bone than MC1288 (*23, 45*). It is tempting to speculate that the increased bone activity of 2MD arises from the different positioning of the side chain brought on by the CD-ring tilt, but the currently available data provide no structural proof.

The fact that 2MbisP is capable of binding to the VDR establishes that the interactions of the 25-OH are not essential for ligand binding. The difference in the biological activity between 2MD and 2MbisP suggests, however, that these interactions may be a determinant of tissue selectivity and/ or potency. The hydrogen bonds formed between the 25-OH and the binding-site histidines assist in positioning the aliphatic side chain and limiting its motion. This action helps
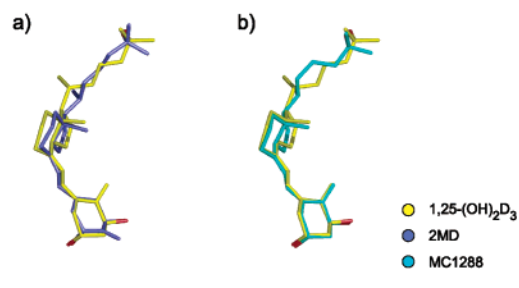
Atoms	Torsion Angle (deg)		
	1,25-(OH)$_2$D$_3$	2MD	MC1288
C13-C17-C20-C22	90	-45	-57
C16-C17-C20-C22	-33	-170	-173
C17-C20-C22-C23	-159	179	178
C20-C22-C23-C24	172	-166	-65
C22-C23-C24-C25	156	173	-167
C23-C24-C24-O25	-68	47	-59

FIGURE 6: Comparison of the CD-ring tilting and side-chain conformations of 2MD and MC1288. (a) Superposition of 1,25-(OH)$_2$D$_3$ and 2MD. (b) Superposition of 1,25-(OH)$_2$D$_3$ and MC1288. These figures were generated after superimposing the protein coordinates of the 2MD- and MC1288-containing structures on those of the rat receptor with the natural ligand. The bottom portion of the figure lists the torsion angles of the 17β-aliphatic side chain in each of the crystal structures.

to define the hydrophobic interactions between the side chain and the protein. The side chain of 2MbisP is shorter and has fewer restrictions upon its motion. As a result, hydrophobic contacts that could be important for biological activity may not be fully realized.

We are, at present, unable to assign a unique function for the 2-methylene moiety of 2MD and 2MbisP. Computational docking experiments with the *E* isomer of 2-ethylidene-19-nor-1α,25-dihydroxyvitamin D$_3$ suggested that the A ring

of this ligand is shifted such that the double bond of the ethylidene group is oriented parallel to the aromatic side chain of Phe 150, allowing increased stabilization of the bound ligand through a π-bond-stacking interaction. The A ring and its surrounding amino acids occupy the same position in each of the crystal structures reported here. With this arrangement, the double bond of the methylene group is unable to form the $\pi-\pi$ interaction with Phe 150 that is predicted by the docking simulations.

The conformational flexibility of the A ring and its effect on biological activity have been the focus of several structure−function studies over the past few decades. The 1α-hydroxyl group on the A ring is essential for receptor binding and biological activity, and Okamura et al. proposed early on that vitamin D dependent calcium regulation requires that this hydroxyl group occupy an equatorial position on the ring (*46*). Our structural determination with the conformationally restricted analogue 2AM20R demonstrates that the ligand binding pocket does indeed exhibit a distinct preference for the equatorially oriented 1α-OH. This finding underscores the importance of the hydrogen-bonding interactions of the 1α-OH with Ser 233 and Arg 270, interactions which would be disrupted with the alternate A-ring conformation. The A-ring strain imposed on 2AM20R by the 2α-methyl group restricts the amount of the β conformer in solution to 6% of the total free ligand. Saturation of the receptor with this conformer is undoubtedly slower than that observed for 1,25-$(OH)_2D_3$; however, the equilibrium dissociation constant for 2AM20R is only 4.6-fold less than that of the natural ligand (*21*), indicating that once bound, the β conformer is held tightly within the binding pocket. On the basis of our structural analysis with 2AM20R, we believe that any ligand possessing a structural modification that completely precludes the formation of the β-chair conformer will not bind to the VDR.

Though the effect of the 2-carbon-substituted ligands on the molecular interaction between the VDR and an intact coactivator protein remains unknown, our studies demonstrate that the nature of the interaction between the receptor and the LXXLL-containing peptide remains constant in each of the complexes. The electrostatic and hydrophobic interactions with the peptide provide significant stabilization of the active receptor conformation, which is evidenced by our inability to grow crystals of the rat VDR−LBD in the absence of the peptide. In the case of the human protein, the active conformation is stabilized by the interaction with the H3n α helix. Though strong hydrogen bonds anchor this helix to the cavity, the hydrophobic contacts within the cavity are less extensive. The ability of this helical peptide to inhibit the binding of known coactivators to the VDR has not been established. The S_{216}VTLELSQL$_{224}$ sequence of the H3n helix corresponds to S_{212}VTLDLSPL$_{220}$ in the rat protein. This latter sequence is disordered in the crystal structures of the rat LBD and does not make the analogous interaction in the coactivator binding pocket. Peptides must bind in the coactivator pocket in a helical conformation so that the necessary hydrophobic and electrostatic interactions are able to form. Our failure to observe an interaction between the S_{212}VTLDLSPL$_{220}$ sequence and the coactivator binding cavity is likely due to the presence of the proline residue at position 219. It is reasonable to expect that this imino acid might disrupt the structure of the helix, which could in turn prevent the formation of a hydrogen bond between the main-chain carbonyl oxygen of Ser 218 and the side chain of Lys 242. Lys 242 and Glu 416 are highly conserved in the ligand binding domain of nuclear receptors (*47*, *48*), and their electrostatic interactions with the main-chain atoms of the coactivator helix appear to be essential for optimal coactivator binding and transactivation. The necessity of these two amino acids for coactivator interaction has been borne out previously by mutagenesis studies with the retinoic acid and estrogen receptors (*47*, *48*).

It has been postulated that the specificity of nuclear receptor−coactivator interactions is determined by the amino acid residues adjacent to the LXXLL sequence (*30*, *44*). In their structural analysis of the PPARγ·SRC-1 complex, Nolte et al. propose that the interaction between the LBD of PPARγ and a coactivator is optimized when a large hydrophobic amino acid is present in the −1 position of the LXXLL sequence (*44*). The side chain of this particular residue binds in a hydrophobic pocket formed by Pro 467 and Leu 468 in helix 12 of the PPARγ−LBD. This type of interaction may also be a determinant for optimal binding to the VDR, since a similar pocket is formed by Pro 412 and Leu 413. The side chain of Met 629, the −1 amino acid of the DRIP 205 NR-2 sequence, is located within this pocket in our crystal structures. The side chain of Val 217, the −1 amino acid in the H3n helix, points into the corresponding pocket in the human VDR (formed by Pro 416 and Leu 417). Because of its small size, Val 217 does not extend as far into this binding pocket, and its interaction is expected to be weaker as a result (the reader should note here that Pro 416 is not displayed in Figure 5b because its distance from Val 217 is greater than 4.0 Å). The nature of the amino acid in the −3 position may also be important for the VDR−coactivator interaction. His 627 occupies this position in DRIP 205, and the crystal structures with the synthetic DRIP 205 peptide show that Nϵ of this residue is approximately 2.6 Å from Nζ of Lys 260. This observation suggests that amino acids that can function as hydrogen-bond acceptors may be preferred in this position.

Though we have gained valuable insight into ligand and coactivator binding, the mechanism of action of 2MD and 2MbisP remains a mystery. However, we have examined only a small fraction of a very large signaling complex. The effect of these ligands on the structure and function of the VDR−DBD is still unknown. Likewise, we do not yet understand how these analogues affect the molecular interactions between the VDR and RXR. These structural determinations are currently being pursued in our laboratory as part of our ongoing effort to delineate the intricate details of vitamin D dependent gene regulation.

REFERENCES

1. Jones, G., Strugnell, S. A., and DeLuca, H. F. (1998) Current understanding of the molecular actions of vitamin D, *Physiol. Rev.* *78*, 1193−1231.

2. Lemire, J. M. (1992) Immunomodulatory role of 1,25-dihydroxy-vitamin D$_3$, *J. Cell. Biochem. 49*, 26−31.

3. Abe, E., Miyaura, C., Sakagami, H., Takeda, M., Konno, K., Yamazaki, T., Yoshiki, S., and Suda, T. (1981) Differentiation of mouse myeloid leukemia cells induced by 1α,25-dihydroxy-vitamin D$_3$, *Proc. Natl. Acad. Sci. U.S.A. 78*, 4990−4994.

4. Tanaka, H., Abe, E., Miyaura, C., Kuribayashi, T., Konno, K., Nishii, Y., and Suda, T. (1982) 1α,25-Dihydroxycholecalciferol and a human myeloid leukemia cell line (HL-60), *Biochem. J. 204*, 713−719.

5. Hosomi, J., Hosoi, J., Abe, E., Suda, T., and Kuroki, T. (1983) Regulation of terminal differentiation of cultured mouse epidermal cells by 1α,25-dihydroxyvitamin D$_3$, *Endocrinology 113*, 1950−1957.

6. Smith, E. L., Walworth, N. C., and Holick, M. F. (1986) Effect of 1α,25-dihydroxyvitamin D$_3$ on the morphologic and biochemical differentiation of cultured human epidermal keratinocytes grown in serum-free conditions, *J. Invest. Dermatol. 86*, 709−714.

7. Slatopolski, E. S., and Brown, A. J. (1997) Vitamin D and renal failure, in *Vitamin D* (Feldman, D., Glorieux, F. H., and Pike, J. W., Eds.) pp 849−865, Academic Press, San Diego, CA.

8. Fraser, D., Kooh, S. W., Kind, H. P., Holick, M. F., Tanaka, Y., and DeLuca, H. F. (1973) Pathogenesis of hereditary vitamin D-dependent rickets. An inborn error of vitamin D metabolism involving defective conversion of 25-hydroxyvitamin D to 1α,25-dihydroxyvitamin D, *N. Engl. J. Med. 289*, 817−822.

9. Glorieux, F. H., Marie, P. J., Pettifor, J. M., and Delvin, E. E. (1980) Bone response to phosphate salts, ergocalciferol, and calcitriol in hypophosphatemic vitamin D-resistant rickets, *N. Engl. J. Med. 303*, 1023−1031.

10. Drezner, M. K. (1997) Clinical disorders of phosphate homeostasis, in *Vitamin D* (Feldman, D., Glorieux, F. H., and Pike, J. W., Eds.) pp 733−753, Academic Press, San Diego, CA.

11. Lamberg-Allardt, C. (1991) Is there a role for vitamin D in osteoporosis? *Calcif. Tissue Int. 49* (Suppl.), S46−49.

12. Langner, A., Verjans, H., Stapor, V., Mol, M., and Fraczykowska, M. (1993) Topical calcitriol in the treatment of chronic plaque psoriasis: a double-blind study, *Br. J. Dermatol. 128*, 566−571.

13. Hayes, C. E. (2000) Vitamin D: a natural inhibitor of multiple sclerosis, *Proc. Nutr. Soc. 59*, 531−535.

14. Bortman, P., Folgueira, M. A., Katayama, M. L., Snitcovsky, I. M., and Brentani, M. M. (2002) Antiproliferative effects of 1,25-dihydroxyvitamin D$_3$ on breast cells: a mini review, *Braz. J. Med. Biol. Res. 35*, 1−9.

15. Konety, B. R., and Getzenberg, R. H. (2002) Vitamin D and prostate cancer, *Urol. Clin. North Am. 29*, 95−106, ix.

16. Massry, S. G., and Goldstein, D. A. (1979) Is calcitriol [1,25-(OH)$_2$D$_3$] harmful to renal function? *JAMA 242*, 1875−1876.

17. Osborn, J. L., Schwartz, G. G., Smith, D. C., Bahnson, R., Day, R., and Trump, D. L. (1995) Phase II trial of oral 1,25-dihydroxyvitamin D (calcitriol) in hormone refractory prostate cancer, *Urol. Oncol. 1*, 195−198.

18. Bouillon, R., Okamura, W. H., and Norman, A. W. (1995) Structure−function relationships in the vitamin D endocrine system, *Endocr. Rev. 16*, 200−257.

19. Ikekawa, N. (1987) Structures and biological activities of vitamin D metabolites and their analogs, *Med. Res. Rev. 7*, 333−366.

20. Nishii, Y., and Okano, T. (2001) History of the development of new vitamin D analogs: studies on 22-oxacalcitriol (OCT) and 2β-(3-hydroxypropoxy)calcitriol (ED-71), *Steroids 66*, 137−146.

21. Sicinski, R. R., Prahl, J. M., Smith, C. M., and DeLuca, H. F. (1998) New 1α,25-dihydroxy-19-norvitamin D$_3$ compounds of high biological activity: synthesis and biological evaluation of 2-hydroxymethyl, 2-methyl, and 2-methylene analogues, *J. Med. Chem. 41*, 4662−4674.

22. Sicinski, R. R., Rotkiewicz, P., Kolinski, A., Sicinska, W., Prahl, J. M., Smith, C. M., and DeLuca, H. F. (2002) 2-Ethyl and 2-ethylidene analogues of 1α,25-dihydroxy-19-norvitamin D$_3$: synthesis, conformational analysis, biological activities, and docking to the modeled rVDR ligand binding domain, *J. Med. Chem. 45*, 3366−3380.

23. Shevde, N. K., Plum, L. A., Clagett-Dame, M., Yamamoto, H., Pike, J. W., and DeLuca, H. F. (2002) A potent analog of 1α,25-dihydroxyvitamin D$_3$ selectively induces bone formation, *Proc. Natl. Acad. Sci. U.S.A. 99*, 13487−13491.

24. Ross, T. K., Prahl, J. M., and DeLuca, H. F. (1991) Overproduction of rat 1,25-dihydroxyvitamin D$_3$ receptor in insect cells using the baculovirus expression system, *Proc. Natl. Acad. Sci. U.S.A. 88*, 6555−6559.

25. MacDonald, P. N., Haussler, C. A., Terpening, C. M., Galligan, M. A., Reeder, M. C., Whitfield, G. K., and Haussler, M. R. (1991) Baculovirus-mediated expression of the human vitamin D receptor. Functional characterization, vitamin D response element interactions, and evidence for a receptor auxiliary factor, *J. Biol. Chem. 266*, 18808−18813.

26. Kimmel-Jehan, C., Jehan, F., and DeLuca, H. F. (1997) Salt concentration determines 1,25-dihydroxyvitamin D$_3$ dependency of vitamin D receptor-retinoid X receptor-vitamin D-responsive element complex formation, *Arch. Biochem. Biophys. 341*, 75−80.

27. Masuyama, H., Brownfield, C. M., St-Arnaud, R., and MacDonald, P. N. (1997) Evidence for ligand-dependent intramolecular folding of the AF-2 domain in vitamin D receptor-activated transcription and coactivator interaction, *Mol. Endocrinol. 11*, 1507−1517.

28. Renaud, J. P., Rochel, N., Ruff, M., Vivat, V., Chambon, P., Gronemeyer, H., and Moras, D. (1995) Crystal structure of the RAR-gamma ligand-binding domain bound to all-trans retinoic acid, *Nature 378*, 681−689.

29. Rachez, C., and Freedman, L. P. (2000) Mechanisms of gene regulation by vitamin D$_3$ receptor: a network of coactivator interactions, *Gene 246*, 9−21.

30. Darimont, B. D., Wagner, R. L., Apriletti, J. W., Stallcup, M. R., Kushner, P. J., Baxter, J. D., Fletterick, R. J., and Yamamoto, K. R. (1998) Structure and specificity of nuclear receptor-coactivator interactions, *Genes Dev. 12*, 3343−3356.

31. Rochel, N., Wurtz, J. M., Mitschler, A., Klaholz, B., and Moras, D. (2000) The crystal structure of the nuclear receptor for vitamin D bound to its natural ligand, *Mol. Cell 5*, 173−179.

32. Tocchini-Valentini, G., Rochel, N., Wurtz, J. M., Mitschler, A., and Moras, D. (2001) Crystal structures of the vitamin D receptor complexed to superagonist 20-epi ligands, *Proc. Natl. Acad. Sci. U.S.A. 98*, 5491−5496.

33. Rachez, C., Gamble, M., Chang, C. P., Atkins, G. B., Lazar, M. A., and Freedman, L. P. (2000) The DRIP complex and SRC-1/p160 coactivators share similar nuclear receptor binding determinants but constitute functionally distinct complexes, *Mol. Cell. Biol. 20*, 2718−2726.

34. Dame, M. C., Pierce, E. A., and DeLuca, H. F. (1985) Identification of the porcine intestinal 1,25-dihydroxyvitamin D$_3$ receptor on sodium dodecyl sulfate/polyacrylamide gels by renaturation and immunoblotting, *Proc. Natl. Acad. Sci. U.S.A. 82*, 7825−7829.

35. Collaborative Computational Project, Number 4. (1994) The CCP4 suite: programs for protein crystallography, *Acta Crystallogr., Sect. D 50*, 760−763.

36. Vagin, A., and Teplyakov, A. (1997) MOLREP: an automated program for molecular replacement, *J. Appl. Crystallogr. 30*, 1022−1025.

37. Murshudov, G. N., Vagin, A. A., and Dodson, E. J. (1997) Refinement of macromolecular structures by the maximum-likelihood method, *Acta Crystallogr., Sect. D 53*, 240−255.

38. Roussel, A., and Cambillau, C. (1991) TURBO FRODO, in *Silicone Graphics Geometry Partners Directory*, p 86, Silicone Graphics, Mountain View, CA.

39. Laskowski, R. A., MacArthur, M. W., Moss, D. S., and Thornton, J. M. (1993) PROCHECK: a program to check the stereochemical quality of protein structure coordinates, *J. Appl. Crystallogr. 26*, 283−291.

40. Kabsch, W. (1976) A solution for the best rotation to relate two sets of vectors, *Acta Crystallogr., Sect. A 32*, 922−923.

41. Wing, R. M., Okamura, W. H., Rego, A., Pirio, M. R., and Norman, A. W. (1975) Studies on vitamin D and its analogs. VIII. Solution conformations of vitamin D$_3$ and 1α,25-dihydroxyvitamin D$_3$ by high-resolution proton magnetic resonance spectroscopy, *J. Am. Chem. Soc. 97*, 4980−4985.

42. Lee, B., and Richards, F. M. (1971) The interpretation of protein structures: estimation of static accessibility, *J. Mol. Biol. 55*, 379−400.

43. Chothia, C. (1975) Structural invariants in protein folding, *Nature 254*, 304−308.

44. Nolte, R. T., Wisely, G. B., Westin, S., Cobb, J. E., Lambert, M. H., Kurokawa, R., Rosenfeld, M. G., Willson, T. M., Glass, C. K., and Milburn, M. V. (1998) Ligand binding and co-activator

assembly of the peroxisome proliferator-activated receptor-gamma, *Nature 395*, 137−143.

45. Binderup, L., Latini, S., Binderup, E., Bretting, C., Calverley, M., and Hansen, K. (1991) 20-epi-vitamin D₃ analogues: a novel class of potent regulators of cell growth and immune responses, *Biochem. Pharmacol. 42*, 1569−1575.

46. Okamura, W. H., Norman, A. W., and Wing, R. M. (1974) Vitamin D: concerning the relationship between molecular topology and biological function, *Proc. Natl. Acad. Sci. U.S.A. 71*, 4194−4197.

47. Henttu, P. M., Kalkhoven, E., and Parker, M. G. (1997) AF-2 activity and recruitment of steroid receptor coactivator-1 to the estrogen receptor depend on a lysine residue conserved in nuclear receptors, *Mol. Cell. Biol. 17*, 1832−1839.

48. Durand, B., Saunders, M., Gaudon, C., Roy, B., Losson, R., and Chambon, P. (1994) Activation function 2 (AF-2) of retinoic acid receptor and 9-cis retinoic acid receptor: presence of a conserved autonomous constitutive activating domain and influence of the nature of the response element on AF-2 activity, *EMBO J. 13*, 5370−5382.

49. Bourguet, W., Ruff, M., Chambon, P., Gronemeyer, H., and Moras, D. (1995) Crystal structure of the ligand-binding domain of the human nuclear receptor RXR-alpha, *Nature 375*, 377−382.

50. DeLano, W. L. (2002) *The PyMOL molecular graphics system*, DeLano Scientific, San Carlos, CA.